Ultra-strong optical harmonic generations in layered platinum disulfide in the mid-infrared

Song Zhu[1,‡], Ruihuan Duan[2,4,‡], Wenduo Chen[1], Fakun Wang[1], Jiayue Han[1], Xiaodong Xu[5], Lishu Wu[2], Ming Ye[1], Fangyuan Sun[1], Song Han[1], Xiaoxu Zhao[2], Chuan Seng Tan[1], Houkun Liang[6], Zheng Liu[1,2,4,*], Qi Jie Wang[1,3,4,*]

[1]School of Electrical and Electronic Engineering, Nanyang Technological University, 639798, Singapore

[2]School of Material Science and Engineering, Nanyang Technological University, 639798, Singapore

[3]School of Physical and Mathematical Sciences, Nanyang Technological University, 637371, Singapore

[4]CINTRA CNRS/NTU/THALES, UMI 3288, Research Techno Plaza, Nanyang Technological University, 637371, Singapore

[5]School of Materials Science and Engineering, Harbin Institute of Technology, Harbin 150001, P. R. China

[6]School of Electronics and Information Engineering, Sichuan University, Chengdu, Sichuan 610064, P. R. China

[‡]These authors contributed equally to this work

*Corresponding authors: qjwang@ntu.edu.sg and z.liu@ntu.edu.sg

Abstract

Nonlinear optical activities (e.g., harmonic generations) in two dimensional (2D) layered materials have attracted much attention due to the great promise in diverse optoelectronic applications such as nonlinear optical modulators, nonreciprocal optical device, and nonlinear optical imaging. Exploration of nonlinear optical response (e.g., frequency conversion) in the infrared, especially the mid-infrared (MIR) region, is highly desirable for ultrafast MIR laser applications ranging from tunable MIR coherent sources, MIR supercontinuum generation, MIR frequency-comb-based spectroscopy to high harmonic generation. However, nonlinear optical effects in 2D layered materials under MIR pump are rarely reported, mainly due to the lack of suitable 2D layered

materials. Van der Waals layered platinum disulfide (PtS_2) with a sizable bandgap from the visible to the infrared region is a promising candidate for realizing MIR nonlinear optical devices. In this work, we investigate the nonlinear optical properties including third-and fifth-harmonic generation (THG and FHG) in thin layered PtS_2 under infrared pump (1550-2510 nm). Strikingly, the ultra-strong third-order nonlinear susceptibility $\chi^{(3)}\left(-3\omega;\omega,\omega,\omega\right)$ of thin layered PtS_2 in the MIR region was estimated to be over 10^{-18} m^2/V^2, which is about one order of that in traditional transition metal chalcogenides. Such excellent performance makes air-stable PtS_2 a potential candidate for developing next-generation MIR nonlinear photonic devices.

Keywords: Mid-infrared, 2D materials, platinum disulfide, nonlinear optics, optical harmonic generation

Nonlinear optical activities, such as harmonic generation, are of importance for various applications including frequency conversion,[1] laser technology[2,3] and optical spectroscopy.[4,5] Nonlinear optical materials for nonlinear optical response (e.g., frequency conversion) in the infrared especially the mid-infrared (MIR) region are highly desirable due to the emergence of ultrafast MIR laser applications including tunable MIR coherent sources,[3] MIR supercontinuum generation,[6] MIR frequency-comb-based spectroscopy[7] and high harmonic generation.[8] Two dimensional (2D) van der Waals layered materials have attracted much attention due to their high nonlinear susceptibilities,[9-19] good compatibility with nanoscale photonic devices[20-24] and tunable optical nonlinearity.[25-32] Harmonic generations in 2D layered materials such as graphene and transition metal chalcogenides (TMDs) have been widely studied in recent years.[1,33-40] However, most of nonlinear optical responses in 2D layered materials are focused in the visible to near infrared (NIR) region. Few attentions have been paid to the MIR region, mainly due to the lack of suitable 2D layered materials. Black phosphorus (BP) possesses layer-dependent direct bandgaps covering the visible to MIR spectral regions.[41] However, BP is not stable in air, which leads to rapid degradation in ambient environment. Graphene has a giant third-order nonlinear susceptibility ($\chi^{(3)}\left(-3\omega;\omega,\omega,\omega\right)$, called $\chi^{(3)}$) in the MIR region (8×10^{-17} m^2/V^2 at ~3100 nm),[33] but graphene suffers from intrinsic limitations for on-off ratio in electronic and photonics devices due to its zero-bandgap nature. Van der Waals layered platinum disulfide (PtS_2), as one kind of group-10 TMDs similar to $PtSe_2$,[42] $PdSe_2$,[43] and $PtTe_2$,[44] demonstrates great potential for optoelectronic applications due to its high carrier mobility,[45] widely tunable bandgap (Figure S1 in the Supporting Information),[46,47] and high stability. Studying the nonlinear optical activity of layered PtS_2 in the infrared region (especially MIR region) is an essential step toward the development of next-generation MIR nonlinear photonic devices. Up to now, there are few works that studied the nonlinear absorption effect in layered PtS_2,[48-50] corresponding to the imaginary part of its third-order nonlinear susceptibility ($\mathrm{Im}\,\chi^{(3)}(\omega;-\omega,\omega,\omega)$). However, up to now, there still lacks experimental investigation of harmonic generations in 2D layered PtS_2.

In this work, we report optical harmonic generations including THG and fifth-harmonic generation (FHG) in 2D layered PtS_2 under NIR to MIR pump (1550 nm-2510 nm). We find that the thin layered PtS_2 flake exhibits ultra-strong $\chi^{(3)}$ values of over 10^{-18} m^2/V^2 under MIR pump,

which is about one order of that in traditional TMDs (e.g., MoS_2, WS_2). In addition, FHG is also observed in layered PtS_2 under MIR pump (2510 nm). These findings not only reveal the intrinsic nonlinear optical properties of PtS_2, but also possess a potential for developing nonlinear optoelectronic devices in the NIR to MIR regions.

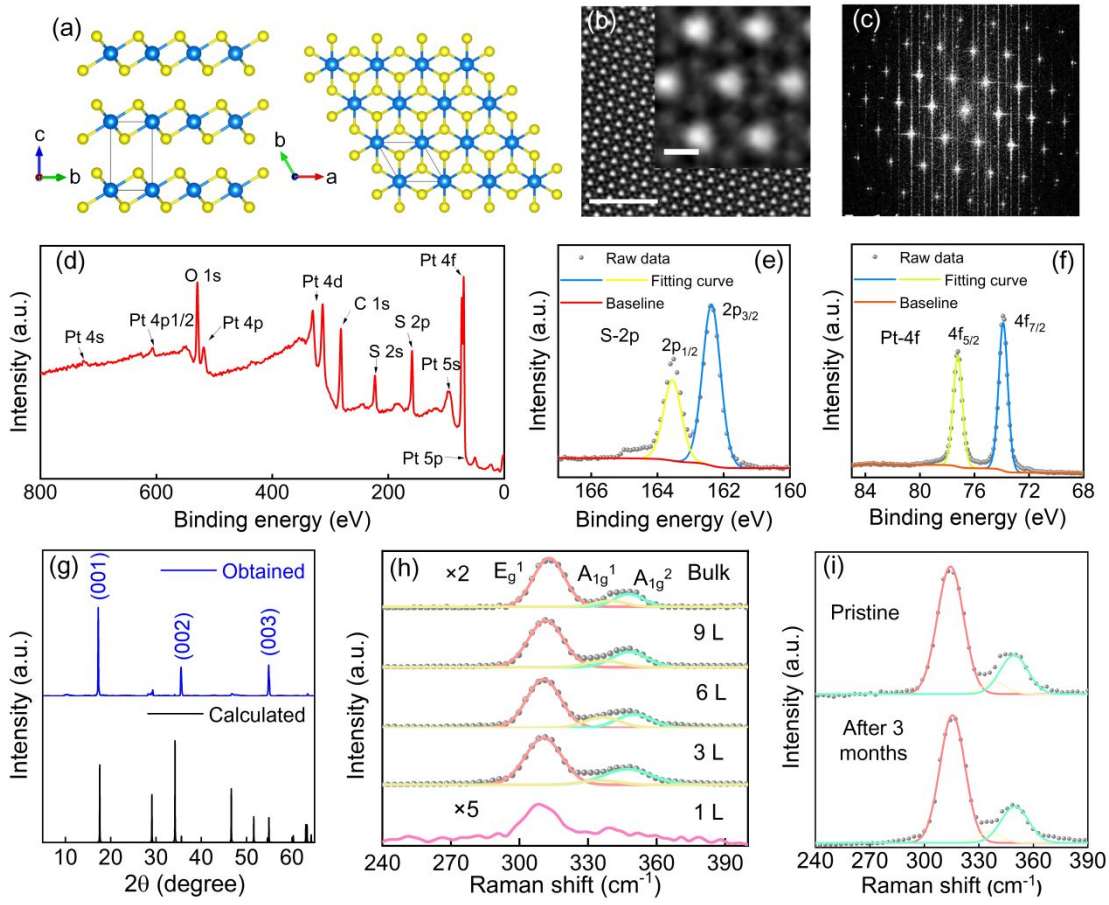

Figure 1. Electron and phonon characterization of the PtS_2 crystal. (a) The crystal structure of PtS_2 with side (left) and top (right) views. (b) The HRTEM image of the thin PtS_2 flake. Scale bar: 2 nm. Inset: an enlarged area of Figure 1 (b). Scale bar: 0.2 nm. (c) The fast Fourier transform (FFT) diffraction patterns. (d) XPS of the PtS_2 flake. (e) S-2p core level, (f) Pt-4f core level. (g) The XRD pattern of the PtS_2 flake. Upper: obtained; bottom: calculated. (h) Raman spectra of 1 L, 3 L, 6 L, 9 L and bulk PtS_2. (i) Raman spectra of the PtS_2 flake. Upper: pristine; bottom: after 3 months.

Results and Discussion

Crystal structure and characterization of van der Waals layered PtS_2

PtS_2 crystal belongs to $P\bar{3}m1$ space group (No. 164). Figure 1a shows the side-view and top-view of the PtS_2 crystal, which exhibits a tilted and slightly distorted octahedral structure, called 1*T* phase with AA arrangement for stacked layers.[46,51] In this structure, each Pt atom is coordinated

by six S atoms in a tilted octahedral structure, which is different from that of Mo in 2H TMD, such as MoS_2 and WS_2, in which each Mo atom is arranged in the site of a triangular-prismatic site. In the side view, PtS_2 exhibits a crystal structure with a monolayer thickness of 8.6 Å.[46] As shown Figures 1b and 1c, the crystal structure of the layered PtS_2 is verified by high-resolution transmission electron microscopy (HRTEM), showing the 1*T* structure. To further confirm the elemental composition and valence states in the PtS_2 crystal, X-ray photoelectron spectroscopy (XPS) measurement is conducted (Figure 1d), confirming Pt and S element ratio of ~1:2 and the valence of Pt^{4+} and S^{2-}. To further investigate the crystal quality of experimentally prepared PtS_2, X-ray diffraction (XRD) characterization is performed. As shown in Figure 1g, the diffraction pattern exhibits three robust peaks at 18°, 36°, and 55°, corresponding to (001), (002), and (003), suggesting a high crystal quality.[45] The three peaks are well matched with the calculated results shown in the bottom of Figure 1g, suggesting the pure phase. Figure 1h shows the thickness-dependent Raman spectra of 2D layered PtS_2 in 1 L, 3 L, 6 L, 9 L and bulk. For monolayer PtS_2, there is only an apparent E_g^1 phonon mode at 307 cm^{-1}, which is due to the limited number of scattering atoms.[46] E_g^1 phonon mode undergoes a blue shift, and the A_g^1 together with the A_g^2 phonon mode emerge with the increase of the layer number. As mentioned, the PtS_2 crystal has good air-stability, which is important for practical applications. To verify this point, we compare the Raman spectra of a pristine layered PtS_2 flake that is measured at times separated by 3 months. As shown in Figure 1i, the Raman spectrum remains unchanged, confirming its good air-stability.

THG process in thin layered PtS_2 flakes

Optical harmonic generations in layered PtS_2 are measured using a home-built microscopic system (Figure 2 and Methods). Figure 3a shows the optical microscopic image of a thin PtS_2 flake. The average thickness of the PtS_2 flake is measured to be ~12 nm using the atomic force microscopy (AFM), corresponding to a flake with roughly 14 L. Since PtS_2 belongs to $\bar{3}m$ point group with inversion symmetry, it is expected to exhibit only odd-order (e.g., THG) nonlinear optical effects.[52] To measure the THG signal, the PtS_2 flake is illuminated by a 1550-nm laser with a spot size of ~2 μm, generated from an optical parametric amplifier (OPA). Figure 3c illustrates THG spectra measured at different pump powers with the central pump wavelength around 1550 nm. The spectrum of fundamental light measured by a Zolix monochromator integrated with a liquid

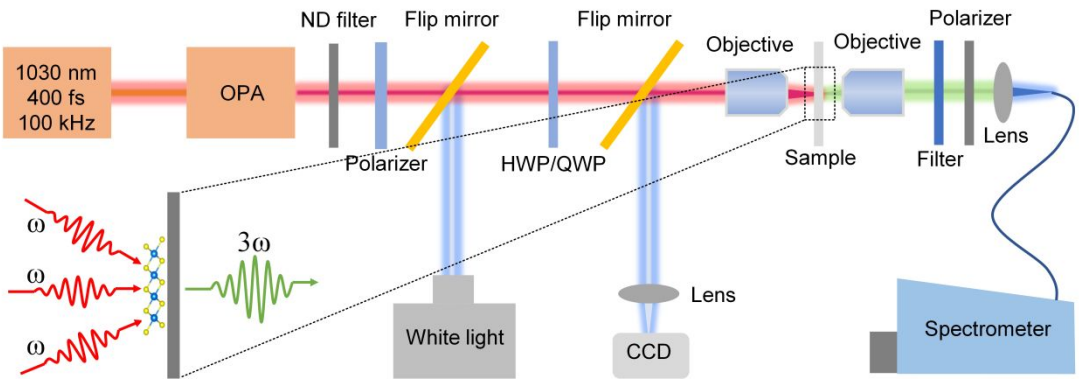

Figure 2. Schematic of the experimental setup. OPA: optical parametric amplifier, ND filter: neutral density filter, HWP: half waveplate, QWP: quarter waveplate. Inset: principle of the THG process.

cooled indium antimonide (InSb) detector is shown in the inset of Figure 3c. The linewidth of the THG spectrum is about 6 nm, which is about three times smaller than that of the fundamental light (~16 nm) due to the nonlinear multiphoton process.[53] Figure 3d shows log-log plot of the THG intensity as a function of the pump power. It can be found that the THG intensity is cubically (slope=3) dependent on the pump power, indicating the THG process. Wavelength-dependent THG in the range from 1515 nm to 1644 nm is also measured and shown in Figures 3e and 3f, showing weak spectral dependence of the THG intensity, indicating a lack of resonance absorption in the PtS_2 flake.[54] Absorption spectra of PtS_2 flakes with thicknesses of 9 nm, 20 nm and 24 nm are also measured (Figure S2 in the Supporting Information), which reveal that there is no clear excitonic transition peak in the visible to MIR region due to the decreased exciton binding energy in the thicker PtS_2 derived from the stronger interlayer interaction and indirect bandgap nature.[46,55]

The polarization angle dependent THG is also measured, as shown in Figure 4a. It can be seen that the THG intensity is independent on the pump polarization, which is due to its $\bar{3}m$ point group for the in-plane symmetry.[52] Besides, the polarization of the THG signal is also measured by rotating a polarizer between the collective objective lens and the spectrometer. Figure 4b shows change of the THG intensity when the polarizer is rotated from 0 to 360°, which indicates the linear polarization characteristic of the THG signal. In addition, the THG polarization is parallel to the polarization of the fundamental light. To clarify its fundamental principle for polarization measurement, we introduce $\chi^{(3)}$ tensor of the PtS_2 crystal. Here, the pump light is linearly

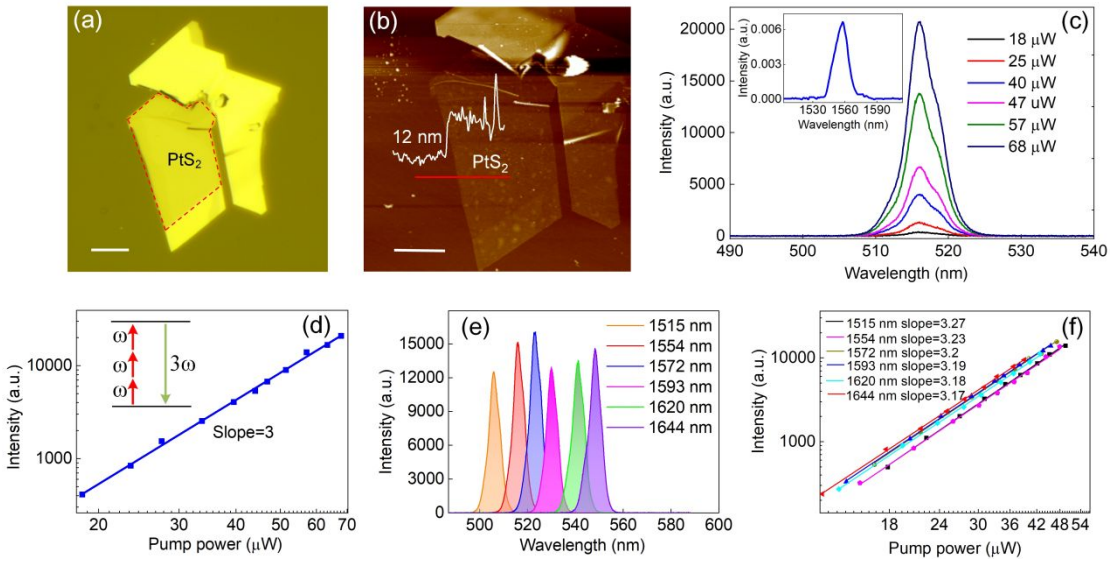

Figure 3. THG processes in the thin layered PtS_2 flake. (a) Optical microscopic image of the PtS_2 flake. Scale bar: 10 μm. (b) The AFM image of the thin PtS_2 flake. Scale bar: 10 μm. (c) THG spectra from the PtS_2 flake depending on the pump power. Inset: 1550-nm pump spectrum. (d) The THG intensity as a function of the pump power. Inset: diagram of the THG process. (e) THG spectra for various pump wavelengths. (f) The THG intensity as a function of the pump power for different pump wavelengths.

polarized with the fundamental frequency ω, which can be expressed as $\mathbf{E} = E_x\mathbf{x} + E_y\mathbf{y} + E_z\mathbf{z}$. A coordinate is assigned in Figure 1a, where the *x*-axis can be along the *a*-axis, the *y*-axis is perpendicular to the *x*-axis, and the *c*-axis is oriented along *z*-axis. Its $\chi^{(3)}$ tensor can be expressed as:[52,56]

$$\begin{bmatrix} \chi_{11} & 0 & 0 & 0 & \chi_{15} & \chi_{16} & -\chi_{15} & 1/3\chi_{11} & 0 & 0 \\ 0 & \chi_{11} & 0 & \chi_{16} & -\chi_{15} & 0 & 0 & 0 & 1/3\chi_{11} & \chi_{15} \\ \chi_{31} & 0 & \chi_{33} & 0 & \chi_{35} & 0 & \chi_{35} & -\chi_{31} & 0 & 0 \end{bmatrix} \quad (1)$$

where the first subscript 1, 2, 3 refers to *x*, *y*, *z*, respectively, and the second subscript refers to the following:

xxx	*yyy*	*zzz*	*yzz*	*yyz*	*xzz*	*xxz*	*xyy*	*xxy*	*xyz*
1	2	3	4	5	6	7	8	9	0

The sample is excited along *z*-axis in our configuration, thus the electric field intensity of the pump light in the *z*-direction can be negligible. Therefore, the pump light can be further expressed as $\mathbf{E} = E_0(\mathbf{x}\cos(\theta) + \mathbf{y}\sin(\theta))$, where θ is the polarization angle relative to the *x*-axis. Therefore, components of the third-order nonlinear polarization ($P^{(3\omega)}$) in the layered PtS_2 crystal can be

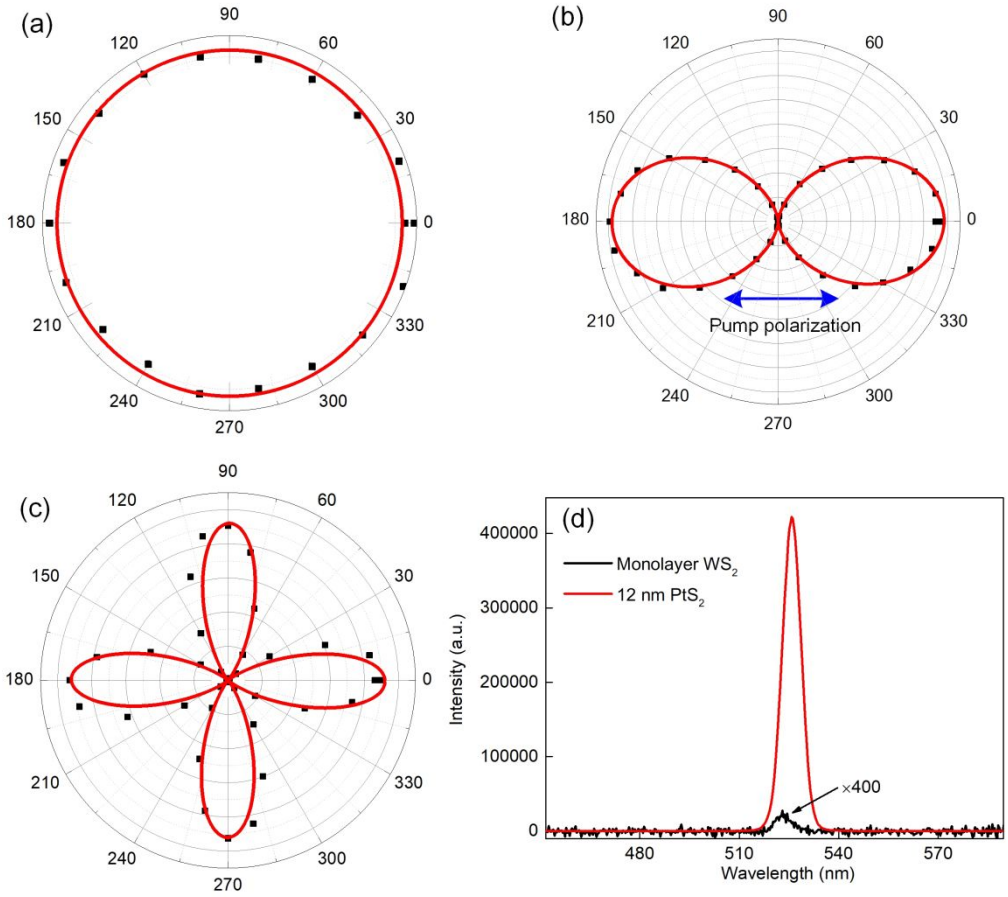

Figure 4. Angle dependent THG in the thin PtS_2 flake. (a) The THG intensity depending on the polarization direction of the linear pump light. (b) The THG intensity versus the rotation angle of the polarizer. (c) The THG intensity depending on the pump ellipsometry. The polar-plot angle corresponds to linearly polarized light when θ = 0°+m·90°, and to circularly polarized light when θ = 45°+m·90°. (d) THG spectra from the thin PtS_2 flake and monolayer WS_2 with the pump power of ~49 μW.

expressed as:

$$P^{(3\omega)} = \begin{bmatrix} P_x^{3\omega} \\ P_y^{3\omega} \\ P_z^{3\omega} \end{bmatrix} = \varepsilon_0 E_0^{\,3} \begin{bmatrix} \chi_{11}\cos^3(\theta) + \chi_{11}\cos(\theta)\sin^2(\theta) \\ \chi_{11}\sin^3(\theta) + \chi_{11}\cos^2(\theta)\sin(\theta) \\ 0 \end{bmatrix} \quad (2)$$

Therefore, the x- and y- components of the THG intensity can be expressed as:

$$\begin{aligned} I_x^{3\omega} &\propto (\chi_{11}\cos^3(\theta) + \chi_{11}\cos(\theta)\sin^2(\theta))^2 \\ I_y^{3\omega} &\propto (\chi_{11}\sin^3(\theta) + \chi_{11}\cos^2(\theta)\sin(\theta))^2 \end{aligned} \quad (3)$$

The total THG intensity $I=I_x+I_y$. The measured polarization resolved THG (Figure 4a) can be well fitted using Eq. (3). Furthermore, the polarization dependent THG for pump light with elliptical polarization is also studied. The electric field intensity of the pump light with the major axis of the

polarization ellipsometry is considered as $\mathbf{E} = E_0\mathbf{e}\pm$, where $\mathbf{e}\pm = \mathbf{x}\cos(\beta) \pm i\mathbf{y}\sin(\beta)$ with β being the ellipticity angle. Therefore, the electric field intensity of the THG signal can be expressed as (for left circular pump):

$$\mathbf{E}^{3\omega} \propto (\chi_{11}\cos^3(\beta) - \chi_{11}\cos(\beta)\sin^2(\beta))\mathbf{x} + i(\chi_{11}\cos^2(\beta)\sin(\beta) - \chi_{11}\sin^3(\beta))\mathbf{y} \quad (4)$$

In Eq. (4), β=0° corresponds to linear polarization, while β=45° corresponds to a circular polarization. The desired elliptical polarization of the pump light is obtained by rotating a quarter waveplate (QWP) working at 1550 nm before being focused on the sample. Here, the ellipticity of the pump light is determined by the angle between the fast axis of QWP and the linearly polarized light. Figure 4c shows polar-plot of the angular dependence of the THG intensity in the layered PtS_2. It can be found that the THG intensity is maximum for a linearly polarized pump, while it becomes almost zero in the case of the circularly polarized pump. The fitted red curve using Eq. (4) agrees well with the experimental data (black dots).

Monolayer WS_2 ($\chi^{(3)} = 2.4\times10^{-19} m^2/V^2$) is used as a reference sample to estimate $\chi^{(3)}$ value of the layered PtS_2.[57] Before doing the estimation, we need to consider whether it will be influenced by the coherent length (l_{coh}). For THG in the bulk materials, there will be phase mismatch ($\Delta k = k_3 - 3k_1 = \frac{6\pi(n_1 - n_3)}{\lambda_1}$) between the fundamental and the forward propagating third-harmonic signal, where k_1 and k_3 are wave vectors of the fundamental and the forward propagating third-harmonic signals, respectively, n_1 and n_3 are refractive indexes (RIs) at fundamental (λ_1) and THG (λ_3) wavelengths, respectively.[58] For layered PtS_2, its RIs at λ_1=1550 nm and λ_3=516 nm are about 3.54 and 3.76, respectively.[59] By calculating using equation: $l_{coh} = |\pi/\Delta k|$,[58] we find that l_{coh} should be about 1174 nm, which is much larger than the flake thickness (12 nm), which means that the phase mismatch cannot influence the THG intensity in our case. For the THG process in the reflective configuration, there is phase mismatch ($\Delta k = k_3 - 3k_1 = \frac{6\pi(n_1 + n_3)}{\lambda_1}$) between the fundamental and the backward propagating third-harmonic signal.[58] Thus, l_{coh} is calculated to be about 35 nm in the reflective configuration, much

smaller than that in the transmission configuration. We only do the transmission measurement since our current setup does not support the reflective configuration. The estimation is performed using the following equation:[60,61]

$$\chi_{PtS_2}^{(3)} = \frac{l_{WS_2}}{l_{PtS_2}} \sqrt{\frac{THG_{PtS_2}}{THG_{WS_2}}} \chi_{WS_2}^{(3)} \quad (5)$$

where THG_{PtS_2/WS_2} are THG intensities of the thin layered PtS_2 flake and monolayer WS_2, respectively, the thickness of monolayer WS_2 (l_{WS_2}) is about 0.67 nm, the thickness of the PtS_2 flake (l_{PtS_2}) is about 12 nm. As shown in Figure 4d, by comparing to monolayer WS_2 (Figure S4), $\chi^{(3)}$ value of PtS_2 is estimated to be about 1.3×10^{-18} m^2/V^2 under 1550-nm pump, which is larger than that in most of 2D materials.

Optical harmonic generations under MIR pump

In addition to the nonlinear response of layered PtS_2 in the NIR region, it would be desirable to further investigate its nonlinear activity in the MIR region (over 2000 nm). Figure 5 shows the THG of the thin layered PtS_2 flake under 2050-nm pump. The thickness of the PtS_2 flake used in this measurement is ~9 nm, as shown in Figure 5a. Figure 5b shows evolution of the THG spectrum with the increase of the pump power. The THG wavelength of around 684 nm corresponds to the pump wavelength of around 2050 nm. As shown in Figure 5c, the linearly fitted slope of ~2.64 verifies the three-photon nonlinear process. Furthermore, its $\chi^{(3)}$ value is also estimated using Eq. (5) by comparing to monolayer graphene (Figure S5).[33] As shown in Figure 5d, $\chi^{(3)}$ value of layered PtS_2 around 2050 nm is estimated to be about 2.7×10^{-18} m^2/V^2 through the spectral measurements for the thin layered PtS_2 flake and monolayer graphene performed with the same pump power of ~100 μW.

In the next step, optical harmonic generation is studied at a pump wavelength of around 2510 nm. As shown in Figure 6a, we can see that THG around 840 nm and FHG around 502 nm are observed with a pump power of ~588 μW. It can be found that the FHG intensity is much smaller than the THG intensity, which is due to a fact that FHG needs the higher pump power.[8,62] Figures

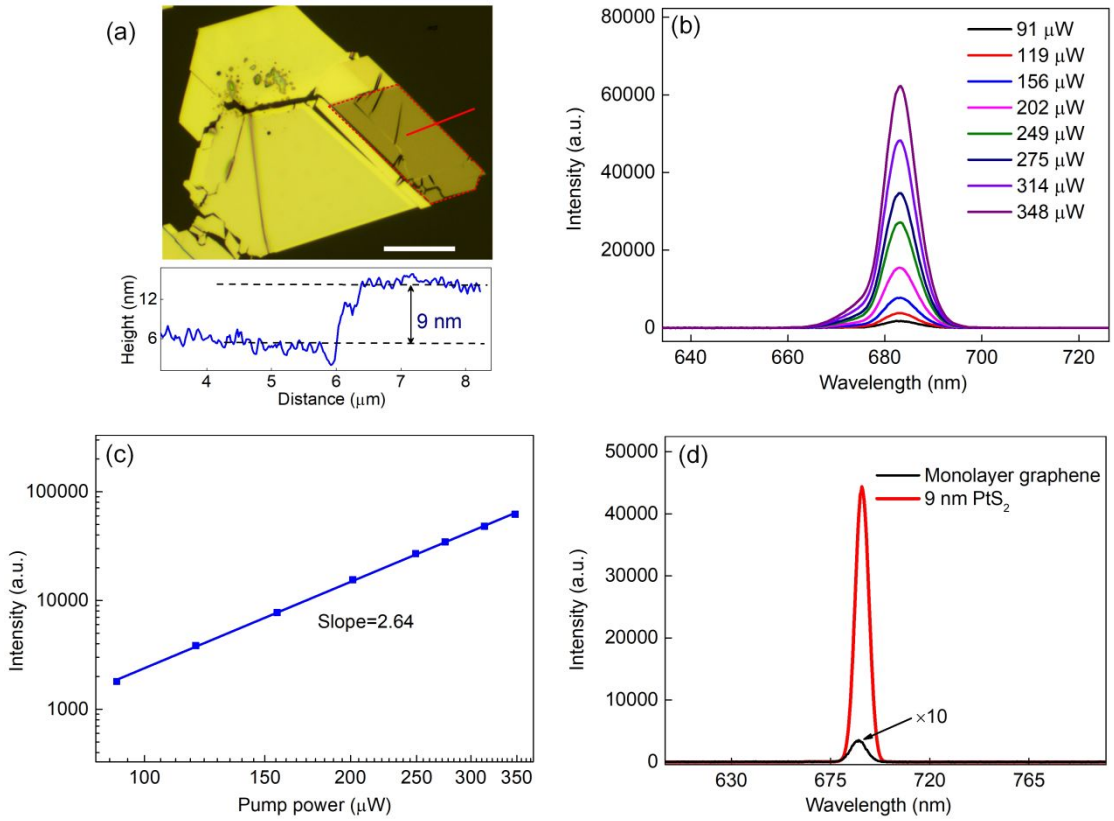

Figure 5. THG of the thin PtS_2 flake under 2050-nm pump. (a) Upper: optical microscopic image of the PtS_2 flake; bottom: AFM measurement result. Scale bar: 30 μm. (b) THG spectra depending on the pump power. (c) The THG intensity as a function of the pump power. (d) THG spectra from the PtS_2 flake and the monolayer graphene measured at the pump power of ~100 μW.

6b and 6c represent evolution of THG and FHG spectra with the increase of the pump power. Furthermore, $\chi^{(3)}$ value around 2510 nm is also estimated by comparing to the monolayer graphene,[33] as shown in Figure 6d. We find that layered PtS_2 has a $\chi^{(3)}$ value of about 2.1×10^{-18} m^2/V^2 in the MIR region. The THG and FHG intensities as a function of the pump power are also measured, as shown in Figure 6e. It can be found that the THG intensity exhibits a nearly cubic dependence on the pump power, but the FHG intensity follows the power dependence of $I^{2.5}$, which shows the non-perturbative character of the HHG process.[8,63] Besides, the THG intensity as a function of the pump power for different thicknesses is plotted in Figure 7a. It is noted that the THG intensity increases as the thickness is increased from 9 nm to 270 nm. However, the intensity decreases when the thickness further increases to 339 nm, which is attributed to the optical

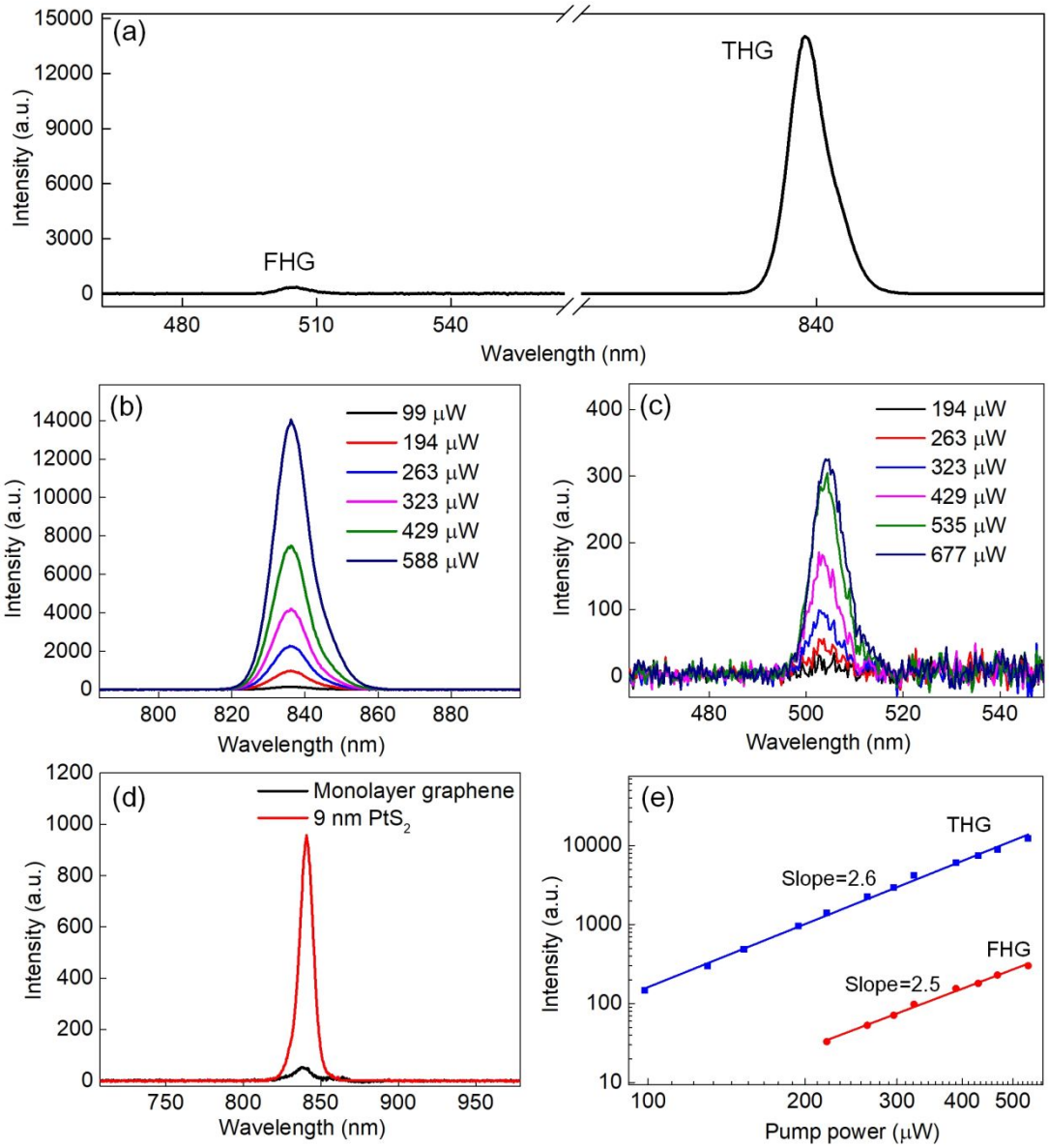

Figure 6. THG and FHG processes of the PtS_2 flake under 2510-nm pump. (a) Typical harmonic generation spectra including THG and FHG. (b) THG spectra depending on the pump power. (c) FHG spectra depending on the pump power. (d) THG spectra of the PtS_2 flake and the monolayer graphene under 2510-nm pump. (e) THG and FHG intensities depending on the pump power.

absorption induced decay when the thickness is large enough.[64] Finally, we also measure $\chi^{(3)}$ value of layered PtS_2 around 1730 nm and 2250 nm, respectively. As shown in Figure 7b, by comparing to the monolayer graphene, layered PtS_2 has $\chi^{(3)}$ values of about 3.3×10^{-18} m^2/V^2 around 1730 nm and about 1.8×10^{-18} m^2/V^2 around 2250 nm, which means that as an air-stable layered material, layered PtS_2 possesses broadband ultra-strong $\chi^{(3)}$ from NIR to MIR regions.

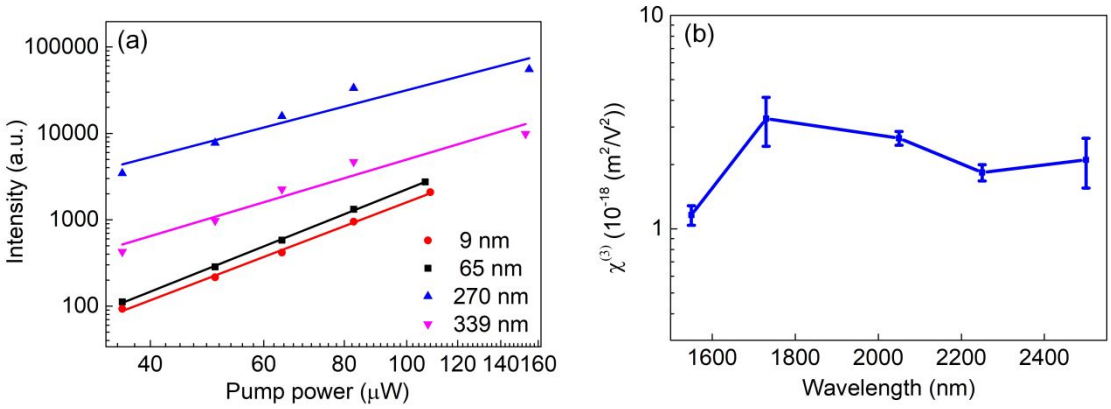

Figure 7. Thickness and wavelength dependent THG processes. (a) Pump power dependent THG intensity with different thicknesses (2510-nm pump). (b) Measured $\chi^{(3)}$ values of the thin layered PtS_2 flakes from NIR to MIR regions.

Comparison of the nonlinear susceptibility of layered PtS_2 with well-studied 2D layered materials and bulk materials is presented in Table 1. It can be found that the nonlinear susceptibility of layered PtS_2 is larger than that in most 2D layered materials and common bulk materials (e.g., Si_3N_4, fused silica). In particular, $\chi^{(3)}$ values of layered PtS_2 are about one order of traditional TMDs, demonstrating that layered PtS_2 is a good candidate for MIR nonlinear photonics. Furthermore, its nonlinear susceptibility is also much larger than that in common bulk materials used in photonic devices, such as Si_3N_4 and fused silica, with good stability in the air. Finally, the nonlinear RI (n_2) of layered PtS_2 is also studied, which is derived from the Kerr nonlinearity, relevant to the real part of the third-order nonlinear susceptibility ($\mathrm{Re}\,\chi^{(3)}(\omega;-\omega,\omega,\omega)$). The nonlinear Kerr effect induced n_2 should be measured by the closed-aperture (CA) Z-scan method.[65] The value of n_2 in layered PtS_2 is up to 1.2×10^{-14} m^2/W at 1030 nm, which is larger than that in most of van der Waals 2D layered materials (Table S1 in the Supporting Information). Based on the measured n_2 at 1030 nm, the $\mathrm{Re}\,\chi^{(3)}(\omega;-\omega,\omega,\omega)$ value of PtS_2 is calculated to be 5.3×10^{-16} m^2/V^2 according to the equation:[66] $n_2(m^2/W)=\frac{3}{4\varepsilon_0 c n_0^2}\mathrm{Re}\,\chi^{(3)}(\omega;-\omega,\omega,\omega)$, where ε_0 is the vacuum permittivity, n_0 is the linear RI and c is the speed of light in a vacuum. The $\mathrm{Re}\,\chi^{(3)}(\omega;-\omega,\omega,\omega)$ value is larger than

$\chi^{(3)}(-3\omega;\omega,\omega,\omega)$ of PtS_2, which is because the band edge absorption of PtS_2 at 1030 nm is much larger than that at the wavelength larger than 1550 nm (Figure S2a in the Supporting Information). In short, both $\mathrm{Re}\,\chi^{(3)}(\omega;-\omega,\omega,\omega)$ and $\chi^{(3)}(-3\omega;\omega,\omega,\omega)$ verify the ultra-strong third-order nonlinear susceptibility of layered PtS_2.

Table 1. Typical $\chi^{(3)}$ values studied by the THG process for low dimensional materials and other common bulk materials used in photonics

Material	$\chi^{(3)}\left(10^{-19} m^2/V^2\right)$	Pump parameters	Ref.
FRP	26.72	1300 nm, 200 fs, 2 kHz	[67]
MoS_2	3.6	1560 nm, 150 fs, 50 MHz	[57]
WS_2	2.4	1560 nm, 150 fs, 50 MHz	[57]
Graphene	800	3100 nm, 150 fs, 80 MHz	[33]
Graphene	50	1771 nm, 150 fs, 80 MHz	[33]
Graphene	1.5	1560 nm, 150 fs, 89 MHz	[68]
BP	1.64	1560 nm, 100 fs, 8 MHz	[69]
hBN	0.084	1064 nm, 150 fs, 80 MHz	[53]
Cd_3As_2	2.3	1560 nm	[70]
Si_3N_4	0.28	1064 nm, 70 ps, 1 kHz	[71]
Fused silica	0.002	1064 nm	[72]
PtS_2	13	1550 nm, 150 fs, 100 kHz	This work
	33	1730 nm, 150 fs, 100 kHz	This work
	21	2510 nm, 150 fs, 100 kHz	This work

FRP: fibrous red phosphorus; BP: black phosphorus; hBN: hexagonal boron nitride

Conclusion

In conclusion, optical harmonic generations including (THG and FHG) of layered PtS_2 from the NIR to MIR regions (1550 nm-2510 nm) are experimentally studied. The layered PtS_2 demonstrates ultra-strong $\chi^{(3)}$ values of over 10^{-18} m^2/V^2 under MIR pump, which is about one order of that in traditional TMDs. Finally, demonstration of high performance fifth-harmonic nonlinear response is also realized in layered PtS_2. We believe van der Waals layered PtS_2 with its good air-stability and large nonlinear responses holds great promise for nonlinear optoelectronic applications including nonlinear wavelength conversion, nonlinear photonic waveguide.

Methods

Sample Preparation

PtS_2 single crystals were synthesized via the chemical vapor transport method. The platinum powder, red phosphorus powder, and sulfur powder with a molar ratio of 1:1:3 were sealed in a silica tube under a high vacuum ($<10^{-2}$ Pa). The sealed tube was loaded in a horizontal furnace, whose reaction zone and growth zone were heated to 800 ℃ and 750 ℃ within one day, respectively. After two weeks, the shiny crystals were obtained in the cold end of the silica tube. The thin PtS_2 flakes were mechanically exfoliated from the bulk crystal. The monolayer WS_2 flakes were exfoliated from bulk WS_2 crystals (2D Semiconductors. USA). The monolayer graphene was obtained by chemical vapor deposition. The characterization of monolayer WS_2 and graphene could be found from part S3 and part S4 in the Supporting Information, respectively.

Sample Characterization

The thicknesses of layered PtS_2 flakes were confirmed through the AFM method. The crystal structure of the exfoliated PtS_2 flakes was studied by HRTEM (JEOL-2100F). The element compositions of the PtS_2 crystal were measured through XPS (Kratos AXIS Supra spectrometer with a dual anode Al Kα (1486.6 eV) X-ray monochromatic source). The XRD patterns were measured using a XRD Bruker D8 Advance Powder with Cu-Kα target at the angle of 5°-60°. The thickness-dependent Raman spectra were collected by a confocal Raman spectrometer (WITec alpha 300 RAS) equipped with a 532-nm laser. The absorption spectra of the layered PtS_2 flakes were measured using a Fourier-transform infrared spectrometer (FTIR) equipped with a silicon detector, an InGaAs detector, and a mercury cadmium telluride (MCT) detector. The micro-absorption measurement was carried out by putting the layered PtS_2 flakes between two aligned reflective objectives for light focusing and collection, respectively. The light was focused on the samples by the objective for the absorption measurement. The absorption spectra were obtained by comparing the transmission spectra between the samples and a substrate.[19]

Experimental Setup

Optical harmonic generations in layered PtS_2 were measured using a home-built optical system, as shown in Figure 2. The sample was excited by an OPA system (pulse width 150 fs, repetition rate 100 kHz). The femtosecond laser beam first passed through a ND filter, a polarizer, and HWP, and then was focused by an objective lens (50×, NA 0.45) to a spot with a diameter of ~2 μm. QWP

was used to generate elliptical light. The MIR pump light was focused by a reflective objective (40×, NA 0.5). The harmonic signals were collected by the other objective lens (20×, NA 0.45), filtered by a short-pass filter, and recorded by a spectrometer integrated with a cooling detector. A polarizer was put after the collective objective lens to check the polarization of the THG signal. Monolayer WS_2 and monolayer graphene were used as references to estimate $\chi^{(3)}(-3\omega;\omega,\omega,\omega)$ value of PtS_2 with the same pump intensity of around 100 GW/cm^2. For example, the pump intensity at 1550 nm for estimation of $\chi^{(3)}(-3\omega;\omega,\omega,\omega)$ is 104 GW/cm^2 and the pump intensity at 2050 nm is 96 GW/cm^2. It is worthy to highlight that $\chi^{(3)}(-3\omega;\omega,\omega,\omega)$ is the intrinsic nonlinear optical property of the materials, which is independent on the pump intensity.

First-Principles Calculations

The strongly constrained and appropriately normed (SCAN) meta-generalized gradient approximation (METAGGA) exchange-correlation potential[73] implemented in VASP package[74] was employed for electronic structure calculations and structural relaxations with a criterion of 0.01 eV/Å. SCAN+rVV10[75] scheme was chosen to accurately evaluate the weak van der Waals interaction among layers. Gamma-centered k-point meshes of 15×15×9 and 15×15×1 were set for bulk and layers, respectively. A cutoff energy of 500 eV was set for all density functional theory (DFT) calculations. Using maximally localized Wannier functions, the Hamiltonian of tight-binding Hamiltonian was constructed using Wannier90 package[76] to reproduce the band structure of DFT.

By solving G0W0 and Bethe-Salpeter equations (BSE) implemented in Yambo code,[77] the layer dependent exciton Bohr radius were evaluated in consideration of the electron-hole interactions for the many body Green's function. In G0W0 calculations, the random integration method was employed and truncated coulomb potential at 32 Å in nonperiodic direction was adopted to avoid problematic image effects in 2D slabs. The plasmon pole approximation was used to obtain of the G0W0 band gap, which was employed in BSE as the scissor operator to avoid the underestimated band gap in usual DFT calculations. The local field effect was also considered with a screening cutoff of 3 Ry.

Supporting Information

Supporting Information is available from online.

Band-structures of PtS_2, linear optical absorption spectra of layered PtS_2 with different thicknesses, optical characterization of monolayer WS_2, optical characterization of monolayer graphene, nonlinear refractive index (n_2) of PtS_2.

Acknowledgements

The authors thank Tingting Wu and Yaze Wu for helpful discussions. This research was also supported partially by National Research Foundation Singapore program (NRF-CRP19-2017-01 and NRF-CRP22-2019-0007) and Ministry of Education Tier 2 program (MOE-T2EP50120-0009), and Singapore A*STAR funding (A18A7b0058 and A2090b0144).

Conflict of Interest

The authors declare no conflict of interest.

References

(1) Zhao, J.; Fieramosca, A.; Bao, R.; Du, W.; Dini, K.; Su, R.; Feng, J.; Luo, Y.; Sanvitto, D.; Liew, T. C. H.; Xiong, Q. Nonlinear Polariton Parametric Emission in an Atomically Thin Semiconductor based Microcavity. *Nat. Nanotechnol.* **2022,** *17*, 396-402.

(2) Liu, J.; Yang, F.; Lu, J.; Ye, S.; Guo, H.; Nie, H.; Zhang, J.; He, J.; Zhang, B.; Ni, Z. High Output Mode-Locked Laser Empowered by Defect Regulation in 2D Bi_2O_2Se Saturable Absorber. *Nat. Commun.* **2022,** *13*, 3855.

(3) Seidel, M.; Xiao, X.; Hussain, S. A.; Arisholm, G.; Hartung, A.; Zawilski, K. T.; Schunemann, P. G.; Habel, F.; Trubetskov, M.; Pervak, V.; Pronin, O.; Krausz, F. Multi-Watt, Multi-Octave, Mid-Infrared Femtosecond Source. *Sci. Adv.* **2018,** *4*, eaaq1526.

(4) Lind, A. J.; Kowligy, A.; Timmers, H.; Cruz, F. C.; Nader, N.; Silfies, M. C.; Allison, T. K.; Diddams, S. A. Mid-Infrared Frequency Comb Generation and Spectroscopy with Few-Cycle Pulses and $\chi^{(2)}$ Nonlinear Optics. *Phys. Rev. Lett.* **2020,** *124*, 133904.

(5) Picqué, N.; Hänsch, T. W. Frequency Comb Spectroscopy. *Nat. Photon.* **2019,** *13*, 146-157.

(6) Chemnitz, M.; Gebhardt, M.; Gaida, C.; Stutzki, F.; Kobelke, J.; Limpert, J.; Tünnermann, A.; Schmidt, M. A. Hybrid Soliton Dynamics in Liquid-Core Fibres. *Nat. Commun.* **2017,** *8*, 42.

(7) Chen, Z.; Hänsch, T. W.; Picqué, N. Mid-Infrared Feed-Forward Dual-Comb Spectroscopy. *Proc. Natl. Acad. Sci.* **2019,** *116*, 3454-3459.

(8) Liu, H.; Li, Y.; You, Y. S.; Ghimire, S.; Heinz, T. F.; Reis, D. A. High-Harmonic Generation from an Atomically Thin Semiconductor. *Nat. Phys.* **2017,** *13*, 262-265.

(9) Ahmed, S.; Jiang, X.; Wang, C.; Kalsoom, U. e.; Wang, B.; Khan, J.; Muhammad, Y.; Duan, Y.; Zhu, H.; Ren, X.; Zhang, H. An Insightful Picture of Nonlinear Photonics in 2D Materials and their Applications: Recent Advances and Future Prospects. *Adv. Opt. Mater.* **2021,** *9*, 2001671.

(10) Autere, A.; Jussila, H.; Dai, Y.; Wang, Y.; Lipsanen, H.; Sun, Z. Nonlinear Optics with 2D Layered Materials. *Adv. Mater.* **2018,** *30*, 1705963.

(11) Ma, R.; Sutherland, D. S.; Shi, Y. Harmonic Generation in Transition Metal Dichalcogenides and their Heterostructures. *Mater. Today* **2021,** *50*, 570-586.

(12) Ahmed, S.; Cheng, P. K.; Qiao, J.; Gao, W.; Saleque, A. M.; Al Subri Ivan, M. N.; Wang, T.; Alam, T. I.; Hani, S. U.; Guo, Z. L.; Yu, S. F.; Tsang, Y. H. Nonlinear Optical Activities in Two-Dimensional Gallium Sulfide: A Comprehensive Study. *ACS Nano* **2022**, *16*, 12390-12402.
(13) Le, C. T.; Kim, J.; Ullah, F.; Nguyen, A. D.; Nguyen Tran, T. N.; Le, T. E.; Chung, K. H.; Cheong, H.; Jang, J. I.; Kim, Y. S. Effects of Interlayer Coupling and Band Offset on Second Harmonic Generation in Vertical $MoS_2/MoS_{2(1-x)}Se_{2x}$ Structures. *ACS Nano* **2020,** *14*, 4366-4373.
(14) Taghizadeh, A.; Thygesen, K. S.; Pedersen, T. G. Two-Dimensional Materials with Giant Optical Nonlinearities Near the Theoretical Upper Limit. *ACS Nano* **2021,** *15*, 7155-7167.
(15) Xiang, Y.; Yan, C.; Stanescu, T. D.; Ma, Y.; Sooriyagoda, R.; Shi, F.; Bristow, A. D.; Li, L.; Cen, C. Giant Third-Harmonic Optical Generation from Topological Insulator Heterostructures. *Nano Lett.* **2021**, *21*, 8872-8879.
(16) Xu, X.; Trovatello, C.; Mooshammer, F.; Shao, Y.; Zhang, S.; Yao, K.; Basov, D. N.; Cerullo, G.; Schuck, P. J. Towards Compact Phase-Matched and Waveguided Nonlinear Optics in Atomically Layered Semiconductors. *Nat. Photon.* **2022,** *16*, 698-706.
(17) Ngo, G. Q.; Najafidehaghani, E.; Gan, Z.; Khazaee, S.; Siems, M. P.; George, A.; Schartner, E. P.; Nolte, S.; Ebendorff-Heidepriem, H.; Pertsch, T.; Tuniz, A.; Schmidt, M. A.; Peschel, U.; Turchanin, A.; Eilenberger, F. In-Fibre Second-Harmonic Generation with Embedded Two-Dimensional Materials. *Nat. Photon.* **2022,** *16*, 769-776.
(18) Dogadov, O.; Trovatello, C.; Yao, B.; Soavi, G.; Cerullo, G. Parametric Nonlinear Optics with Layered Materials and Related Heterostructures. *Laser Photonics Rev.* **2022,** *16*, 2100726.
(19) Abdelwahab, I.; Tilmann, B.; Wu, Y.; Giovanni, D.; Verzhbitskiy, I.; Zhu, M.; Berté, R.; Xuan, F.; Menezes, L. d. S.; Eda, G.; Sum, T. C.; Quek, S. Y.; Maier, S. A.; Loh, K. P. Giant Second-Harmonic Generation in Ferroelectric $NbOI_2$. *Nat. Photon.* **2022,** *16*, 644-650.
(20) Gu, T.; Petrone, N.; McMillan, J. F.; van der Zande, A.; Yu, M.; Lo, G. Q.; Kwong, D. L.; Hone, J.; Wong, C. W. Regenerative Oscillation and Four-Wave Mixing in Graphene Optoelectronics. *Nat. Photon.* **2012,** *6*, 554-559.
(21) Hu, G.; Hong, X.; Wang, K.; Wu, J.; Xu, H.-X.; Zhao, W.; Liu, W.; Zhang, S.; Garcia-Vidal, F.; Wang, B.; Lu, P.; Qiu, C. W. Coherent Steering of Nonlinear Chiral Valley Photons with a Synthetic Au-WS_2 Metasurface. *Nat. Photon.* **2019,** *13*, 467-472.
(22) Geler-Kremer, J.; Eltes, F.; Stark, P.; Stark, D.; Caimi, D.; Siegwart, H.; Jan Offrein, B.; Fompeyrine, J.; Abel, S. A Ferroelectric Multilevel Non-Volatile Photonic Phase Shifter. *Nat. Photon.* **2022,** *16*, 491-497.
(23) Datta, I.; Chae, S. H.; Bhatt, G. R.; Tadayon, M. A.; Li, B.; Yu, Y.; Park, C.; Park, J.; Cao, L.; Basov, D. N.; Hone, J.; Lipson, M. Low-Loss Composite Photonic Platform based on 2D Semiconductor Monolayers. *Nat. Photon.* **2020,** *14*, 256-262.
(24) Bernhardt, N.; Koshelev, K.; White, S. J. U.; Meng, K. W. C.; Fröch, J. E.; Kim, S.; Tran, T. T.; Choi, D. Y.; Kivshar, Y.; Solntsev, A. S. Quasi-BIC Resonant Enhancement of Second-Harmonic Generation in WS_2 Monolayers. *Nano Lett.* **2020,** *20*, 5309-5314.
(25) Sun, Z. Electrically Tuned Nonlinearity. *Nat. Photon.* **2018,** *12*, 383-385.
(26) Wang, Y.; Xiao, J.; Chung, T. F.; Nie, Z.; Yang, S.; Zhang, X. Direct Electrical Modulation of Second-Order Optical Susceptibility via Phase Transitions. *Nat. Electron.* **2021,** *4*, 725-730.
(27) Yu, Y.; Yang, F.; Lu, X. F.; Yan, Y. J.; Cho, Y. H.; Ma, L.; Niu, X.; Kim, S.; Son, Y. W.; Feng, D.; Li, S.; Cheong, S. W.; Chen, X. H.; Zhang, Y. Gate-Tunable Phase Transitions in Thin Flakes of 1T-TaS_2. *Nat. Nanotechnol.* **2015,** *10*, 270-276.

(28) Jiang, T.; Huang, D.; Cheng, J.; Fan, X.; Zhang, Z.; Shan, Y.; Yi, Y.; Dai, Y.; Shi, L.; Liu, K.; Zeng, C.; Zi, J.; Sipe, J. E.; Shen, Y. R.; Liu, W. T.; Wu, S. Gate-Tunable Third-Order Nonlinear Optical Response of Massless Dirac Fermions in Graphene. *Nat. Photon.* **2018,** *12*, 430-436.
(29) Kovalev, S.; Hafez, H. A.; Tielrooij, K. J.; Deinert, J. C.; Ilyakov, I.; Awari, N.; Alcaraz, D.; Soundarapandian, K.; Saleta, D.; Germanskiy, S.; Chen, M.; Bawatna, M.; Green, B.; Koppens, F. H. L.; Mittendorff, M.; Bonn, M.; Gensch, M.; Turchinovich, D. Electrical Tunability of Terahertz Nonlinearity in Graphene. *Sci. Adv.* **2021,** *7*, eabf9809.
(30) Yao, K.; Finney, N. R.; Zhang, J.; Moore, S. L.; Xian, L.; Tancogne-Dejean, N.; Liu, F.; Ardelean, J.; Xu, X.; Halbertal, D.; Watanabe, K.; Taniguchi, T.; Ochoa, H.; Asenjo-Garcia, A.; Zhu, X.; Basov, D. N.; Rubio, A.; Dean, C. R.; Hone, J.; Schuck, P. J. Enhanced Tunable Second Harmonic Generation from Twistable Interfaces and Vertical Superlattices in Boron Nitride Homostructures. *Sci. Adv.* **2021,** *7*, eabe8691.
(31) Wang, J.; Han, N.; Luo, Z.-D.; Zhang, M.; Chen, X.; Liu, Y.; Hao, Y.; Zhao, J.; Gan, X. Electrically Tunable Second Harmonic Generation in Atomically Thin ReS_2. *ACS Nano* **2022,** *16*, 6404-6413.
(32) Seyler, K. L.; Schaibley, J. R.; Gong, P.; Rivera, P.; Jones, A. M.; Wu, S.; Yan, J.; Mandrus, D. G.; Yao, W.; Xu, X. Electrical Control of Second-Harmonic Generation in a WSe_2 Monolayer Transistor. *Nat. Nanotechnol.* **2015,** *10*, 407-411.
(33) Soavi, G.; Wang, G.; Rostami, H.; Purdie, D. G.; De Fazio, D.; Ma, T.; Luo, B.; Wang, J.; Ott, A. K.; Yoon, D.; Bourelle, S. A.; Muench, J. E.; Goykhman, I.; Dal Conte, S.; Celebrano, M.; Tomadin, A.; Polini, M.; Cerullo, G.; Ferrari, A. C. Broadband, Electrically Tunable Third-Harmonic Generation in Graphene. *Nat. Nanotechnol.* **2018,** *13*, 583-588.
(34) Ha, S.; Park, N. H.; Kim, H.; Shin, J.; Choi, J.; Park, S.; Moon, J.-Y.; Chae, K.; Jung, J.; Lee, J. H.; Yoo, Y.; Park, J. Y.; Ahn, K. J.; Yeom, D. I. Enhanced Third-Harmonic Generation by Manipulating the Twist Angle of Bilayer Graphene. *Light Sci. Appl.* **2021,** *10*, 1-10..
(35) Saynatjoki, A.; Karvonen, L.; Rostami, H.; Autere, A.; Mehravar, S.; Lombardo, A.; Norwood, R. A.; Hasan, T.; Peyghambarian, N.; Lipsanen, H.; Kieu, K.; Ferrari, A. C.; Polini, M.; Sun, Z. Ultra-Strong Nonlinear Optical Processes and Trigonal Warping in MoS_2 Layers. *Nat Commun* **2017,** *8*, 893.
(36) Wang, Y.; Xiao, J.; Zhu, H.; Li, Y.; Alsaid, Y.; Fong, K. Y.; Zhou, Y.; Wang, S.; Shi, W.; Wang, Y.; Zettl, A.; Reed, E. J.; Zhang, X. Structural Phase Transition in Monolayer $MoTe_2$ Driven by Electrostatic Doping. *Nature* **2017,** *550*, 487-491.
(37) Yu, J.; Kuang, X.; Li, J.; Zhong, J.; Zeng, C.; Cao, L.; Liu, Z.; Zeng, Z.; Luo, Z.; He, T.; Pan, A.; Liu, Y. Giant Nonlinear Optical Activity in Two-Dimensional Palladium Diselenide. *Nat. Commun.* **2021,** *12*, 1083.
(38) Klimmer, S.; Ghaebi, O.; Gan, Z.; George, A.; Turchanin, A.; Cerullo, G.; Soavi, G. All-Optical Polarization and Amplitude Modulation of Second-Harmonic Generation in Atomically Thin Semiconductors. *Nat. Photon.* **2021,** *15*, 837-842.
(39) Hong, H.; Wu, C.; Zhao, Z.; Zuo, Y.; Wang, J.; Liu, C.; Zhang, J.; Wang, F.; Feng, J.; Shen, H.; Yin, J.; Wu, Y.; Zhao, Y.; Liu, K.; Gao, P.; Meng, S.; Wu, S.; Sun, Z.; Liu, K.; Xiong, J. Giant Enhancement of Optical Nonlinearity in Two-Dimensional Materials by Multiphoton-Excitation Resonance Energy Transfer from Quantum Dots. *Nat. Photon.* **2021,** *15*, 510-515.
(40) Yi, F.; Ren, M.; Reed, J. C.; Zhu, H.; Hou, J.; Naylor, C. H.; Johnson, A. T. C.; Agarwal, R.; Cubukcu, E. Optomechanical Enhancement of Doubly Resonant 2D Optical Nonlinearity. *Nano Lett.* **2016,** *16*, 1631-1636.

(41) Li, L.; Kim, J.; Jin, C.; Ye, G. J.; Qiu, D. Y.; da Jornada, F. H.; Shi, Z.; Chen, L.; Zhang, Z.; Yang, F.; Watanabe, K.; Taniguchi, T.; Ren, W.; Louie, S. G.; Chen, X. H.; Zhang, Y.; Wang, F. Optical Properties of Black Phosphorus. *Nat. Nanotechnol.* **2017,** *12*, 21-25.
(42) Yu, X.; Yu, P.; Wu, D.; Singh, B.; Zeng, Q.; Lin, H.; Zhou, W.; Lin, J.; Suenaga, K.; Liu, Z.; Wang, Q. J. Atomically Thin Noble Metal Dichalcogenide: A Broadband Mid-Infrared Semiconductor. *Nat. Commun.* **2018,** *9*, 1545.
(43) Wang, Z.; Xia, H.; Wang, P.; Zhou, X.; Liu, C.; Zhang, Q.; Wang, F.; Huang, M.; Chen, S.; Wu, P.; Chen, Y.; Ye, J.; Huang, S.; Yan, H.; Gu, L.; Miao, J.; Li, T.; Chen, X.; Lu, W.; Zhou, P.; *et al.* Controllable doping in 2D layered materials. *Adv. Mater.* **2021,** *33*, 2104942.
(44) Zeng, L.; Wu, D.; Jie, J.; Ren, X.; Hu, X.; Lau, S. P.; Chai, Y.; Tsang, Y. H. Van der Waals Epitaxial Growth of Mosaic-Like 2D Platinum Ditelluride Layers for Room-Temperature Mid-Infrared Photodetection up to 10.6 μm. *Adv. Mater.* **2020,** *32*, 2004412.
(45) Li, L.; Wang, W.; Chai, Y.; Li, H.; Tian, M.; Zhai, T. Few-Layered PtS_2 Phototransistor on h-BN with High Gain. *Adv. Funct. Mater.* **2017,** *27*, 1701011.
(46) Zhao, Y.; Qiao, J.; Yu, P.; Hu, Z.; Lin, Z.; Lau, S. P.; Liu, Z.; Ji, W.; Chai, Y. Extraordinarily Strong Interlayer Interaction in 2D Layered PtS_2. *Adv. Mater.* **2016,** *28*, 2399-2407.
(47) Pi, L.; Li, L.; Liu, K.; Zhang, Q.; Li, H.; Zhai, T. Recent Progress on 2D Noble-Transition-Metal Dichalcogenides. *Adv. Funct. Mater.* **2019,** *29*, 1904932.
(48) Wang, X.; Cheng, P. K.; Tang, C. Y.; Long, H.; Yuan, H.; Zeng, L.; Ma, S.; Qarony, W.; Tsang, Y. H. Laser Q-Switching with PtS_2 Microflakes Saturable Absorber. *Opt. Express* **2018,** *26*, 13055-13060.
(49) Long, H.; Tang, C. Y.; Cheng, P. K.; Wang, X. Y.; Qarony, W.; Tsang, Y. H. Ultrafast Laser Pulses Generation by Using 2D Layered PtS_2 as a Saturable Absorber. *J. Lightwave Technol.* **2019,** *37*, 1174-1179.
(50) Optical MaterialsTang, C. Y.; Cheng, P. K.; Wang, X. Y.; Ma, S.; Long, H.; Tsang, Y. H. Size-Dependent Nonlinear Optical Properties of Atomically Thin PtS_2 Nanosheet. *Opt. Mater.* **2020,** *101*, 109694.
(51) Miró, P.; Ghorbani-Asl, M.; Heine, T. Two Dimensional Materials Beyond MoS_2: Noble-Transition-Metal Dichalcogenides. *Angew. Chem. Int. Ed.* **2014,** *53*, 3015-3018.
(52) Boyd, R. W., *Nonlinear optics*. Academic press, **2020**.
(53) Popkova, A. A.; Antropov, I. M.; Fröch, J. E.; Kim, S.; Aharonovich, I.; Bessonov, V. O.; Solntsev, A. S.; Fedyanin, A. A. Optical Third-Harmonic Generation in Hexagonal Boron Nitride Thin Films. *ACS Photonics* **2021,** *8*, 824-831.
(54) Rodrigues, M. J. L. F.; de Matos, C. J. S.; Ho, Y. W.; Peixoto, H.; de Oliveira, R. E. P.; Wu, H. Y.; Neto, A. H. C.; Viana-Gomes, J. Resonantly Increased Optical Frequency Conversion in Atomically Thin Black Phosphorus. *Adv. Mater.* **2016,** *28*, 10693-10700.
(55) Zhang, G.; Chaves, A.; Huang, S.; Wang, F.; Xing, Q.; Low, T.; Yan, H. Determination of Layer-Dependent Exciton Binding Energies in Few-Layer Black Phosphorus. *Sci. Adv.* **2018,** *4*, eaap9977.
(56) Yang, X. L.; Xie, S. W. Expression of Third-Order Effective Nonlinear Susceptibility for Third-Harmonic Generation in Crystals. *Appl. Opt.* **1995,** *34*, 6130-6135.
(57) Autere, A.; Jussila, H.; Marini, A.; Saavedra, J.; Dai, Y.; Säynätjoki, A.; Karvonen, L.; Yang, H.; Amirsolaimani, B.; Norwood, R. A. Optical Harmonic Generation in Monolayer Group-VI Transition Metal Dichalcogenides. *Phys. Rev. B* **2018,** *98*, 115426.
(58) Youngblood, N.; Peng, R.; Nemilentsau, A.; Low, T.; Li, M. Layer-Tunable Third-Harmonic

Generation in Multilayer Black Phosphorus. *ACS Photonics* **2017,** *4*, 8-14.
(59) Ermolaev, G. A.; Voronin, K. V.; Tatmyshevskiy, M. K.; Mazitov, A. B.; Slavich, A. S.; Yakubovsky, D. I.; Tselin, A. P.; Mironov, M. S.; Romanov, R. I.; Markeev, A. M.; Kruglov, I. A.; Novikov, S. M.; Vyshnevyy, A. A.; Arsenin, A. V.; Volkov, V. S. Broadband Optical Properties of Atomically Thin PtS_2 and $PtSe_2$. *Nanomaterials* **2021,** *11*, 3269.
(60) Susoma, J.; Karvonen, L.; Säynätjoki, A.; Mehravar, S.; Norwood, R. A.; Peyghambarian, N.; Kieu, K.; Lipsanen, H.; Riikonen, J. Second and Third Harmonic Generation in Few-Layer Gallium Telluride Characterized by Multiphoton Microscopy. *Appl. Phys. Lett.* **2016,** *108*, 073103.
(61) Karvonen, L.; Säynätjoki, A.; Mehravar, S.; Rodriguez, R. D.; Hartmann, S.; Zahn, D. R. T.; Honkanen, S.; Norwood, R. A.; Peyghambarian, N.; Kieu, K.; Lipsanen, H.; Riikonen, J. Investigation of Second-and Third-Harmonic Generation in Few-Layer Gallium Selenide by Multiphoton Microscopy. *Sci. Rep.* **2015,** *5*, 10334.
(62) Lv, Y. Y.; Xu, J.; Han, S.; Zhang, C.; Han, Y.; Zhou, J.; Yao, S. H.; Liu, X. P.; Lu, M. H.; Weng, H.; Xie, Z.; Chen, Y. B.; Hu, J.; Chen, Y. F.; Zhu, S. High-Harmonic Generation in Weyl Semimetal β-WP_2 Crystals. *Nat. Commun.* **2021,** *12*, 6437.
(63) Yoshikawa, N.; Tamaya, T.; Tanaka, K. High-Harmonic Generation in Graphene Enhanced by Elliptically Polarized Light Excitation. *Science* **2017,** *356*, 736-738.
(64) Sar, H.; Gao, J.; Yang, X. 2D Layered SiP as Anisotropic Nonlinear Optical Material. *Sci. Rep.* **2021,** *11*, 6372.
(65) Zheng, X.; Jia, B.; Chen, X.; Gu, M. In Situ Third-Order Non-linear Responses During Laser Reduction of Graphene Oxide Thin Films Towards On-Chip Non-linear Photonic Devices. *Adv. Mater.* **2014,** *26*, 2699-2703.
(66) Yang, T.; Abdelwahab, I.; Lin, H.; Bao, Y.; Rong Tan, S. J.; Fraser, S.; Loh, K. P.; Jia, B. Anisotropic Third-Order Nonlinearity in Pristine and Lithium Hydride Intercalated Black Phosphorus. *ACS Photonics* **2018,** *5*, 4969-4977.
(67) Du, L.; Zhao, Y.; Wu, L.; Hu, X.; Yao, L.; Wang, Y.; Bai, X.; Dai, Y.; Qiao, J.; Uddin, M. G.; Li, X.; Lahtinen, J.; Bai, X.; Zhang, G.; Ji, W.; Sun, Z. Giant Anisotropic Photonics in the 1D Van der Waals Semiconductor Fibrous Red Phosphorus. *Nat. Commun.* **2021,** *12*, 4822.
(68) Woodward, R. I.; Murray, R. T.; Phelan, C. F.; Oliveira, R. E. P. d.; Runcorn, T. H.; Kelleher, E. J. R.; Li, S.; Oliveira, E. C. d.; Fechine, G. J. M.; Eda, G.; Matos, C. J. S. d. Characterization of the Second- and Third-Order Nonlinear Optical Susceptibilities of Monolayer MoS_2 using Multiphoton Microscopy. *2D Materials* **2016,** *4*, 011006.
(69) Autere, A.; Ryder, C. R.; Säynätjoki, A.; Karvonen, L.; Amirsolaimani, B.; Norwood, R. A.; Peyghambarian, N.; Kieu, K.; Lipsanen, H.; Hersam, M. C.; Sun, Z. Rapid and Large-Area Characterization of Exfoliated Black Phosphorus using Third-Harmonic Generation Microscopy. *J. Phys. Chem. C* **2017,** *8*, 1343-1350.
(70) Ullah, K.; Meng, Y.; Sun, Y.; Yang, Y.; Wang, X.; Wang, A.; Wang, X.; Xiu, F.; Shi, Y.; Wang, F. Third harmonic generation in Dirac semimetal Cd_3As_2. *Appl. Phys. Lett.* **2020,** *117*, 011102.
(71) Ning, T.; Hyvärinen, O.; Pietarinen, H.; Kaplas, T.; Kauranen, M.; Genty, G. Third-harmonic UV Generation in Silicon Nitride Nanostructures. *Opt. Express* **2013,** *21*, 2012-2017.
(72) Gubler, U.; Bosshard, C. Optical Third-Harmonic Generation of Fused Silica in Gas Atmosphere: Absolute Value of the Third-Order Nonlinear Optical Susceptibility $\chi^{(3)}$. *Phys. Rev. B* **2000,** *61*, 10702.
(73) Sun, J.; Ruzsinszky, A.; Perdew, J. P. Strongly Constrained and Appropriately Normed Semilocal Density Functional. *Phys. Rev. Lett.* **2015,** *115*, 036402.

(74) Kresse, G.; Furthmüller, J. Efficient Iterative Schemes for ab Initio Total-Energy Calculations using a Plane-Wave Basis Set. *Phys. Rev. B* **1996,** *54*, 11169.
(75) Peng, H.; Yang, Z. H.; Perdew, J. P.; Sun, J. Versatile Van der Waals Density Functional based on a Meta-Generalized Gradient Approximation. *Phys. Rev. X* **2016,** *6*, 041005.
(76) Mostofi, A. A.; Yates, J. R.; Lee, Y. S.; Souza, I.; Vanderbilt, D.; Marzari, N. Wannier90: A Tool for Obtaining Maximally-Localised Wannier Functions. *Comput. Phys. Commun.* **2008,** *178*, 685-699.
(77) Marini, A.; Hogan, C.; Grüning, M.; Varsano, D. Yambo: An ab Initio Tool for Excited State Calculations. *Comput. Phys. Commun.* **2009,** *180*, 1392-1403.

TOC for the manuscript